RESEARCH ON THE INTEGRATED NAVIGATION AND POSITIONING SYSTEM FOR POWER CHASSIS IN HILLY AND MOUNTAINOUS AREAS BASED ON PPP-RTK/IMU

/ 基于 PPP-RTK/IMU 的丘陵山区动力底盘组合导航定位系统研究

Weisong ZHAO[1)], Binxing XU[1)], Chunsong GUAN[1*)], Jia DENG[2)], Jian WU[2)], Haiyong REN[3)], Jinlong WANG[3)], Shen ZHANG[4)], Zhifeng CHEN[4)]

[1)] Nanjing Institute of Agricultural Mechanization, Ministry of Agriculture and Rural Affairs, Nanjing 210014, China
[2)] Sichuan Academy of Agricultural Machinery Sciences, Chengdu，610066, China
[3)] Jiangsu Yueda Intelligent Agricultural Equipment Co.Ltd, Yancheng 224007, China
[4)] China National Tobacco Corporation Hunan Provincial Company, Changsha 410000, China
Tel: +86025-84346161; E-mail: wszhao77@163.com, cs.guan@163.com
** Correspondent authors: Chunsong Guan*

DOI: https://doi.org/10.35633/inmateh-77-70

Keywords: *Hilly and Mountainous Areas, Power Chassis, PPP-RTK, Navigation, Positioning, Kalman Filter*

ABSTRACT

To address the issue that single-satellite navigation systems are prone to signal occlusion and weakening, resulting in insufficient positioning accuracy when power chassis equipment operates in hilly and mountainous areas, a combined navigation scheme integrating Precise Point Positioning (PPP), Real-Time Kinematic (RTK), and an Inertial Measurement Unit (IMU) was proposed. A simulation model was developed using the PSINS (Precision Strapdown Inertial Navigation System) toolbox within the MATLAB environment. A straight-line trajectory was designed to simulate weakly nonlinear operating conditions, while a circular trajectory was used to represent the strong nonlinear continuous-turning conditions. The performance of the Extended Kalman Filter (EKF) was compared with that of the Unscented Kalman Filter (UKF). A combined PPP-RTK-IMU navigation test system was constructed, and both field experiments and verification tests were conducted in hilly and mountainous regions. The results showed that, in the circular trajectory simulation, the standard deviations of eastward, northward, and vertical position errors obtained using the UKF were reduced by 22%, 19%, and 18%, respectively, compared with those of the EKF. In field tests, the UKF demonstrated significantly better consistency with the reference values than the EKF. Results from five repeated field verification tests showed that the average maximum absolute lateral position deviation was 10.96 cm, the mean absolute deviation averaged 3.08 cm, and the average standard deviation was 3.02 cm, all meeting operational requirements. Overall, the findings indicate that the UKF is more suitable for strongly nonlinear operating scenarios encountered in hilly and mountainous terrain, and that the proposed combined navigation system effectively mitigates satellite signal occlusion, thereby meeting the precision requirements of modern agricultural machinery operations.

摘要

针对丘陵山区动力底盘作业时单一卫星导航易受遮挡、信号弱导致定位精度不足的问题，提出精密单点定位（PPP）-实时动态差分（RTK）与惯性测量单元（IMU）深度融合的组合导航方案。基于 MATLAB 平台的 PSINS 惯性导航工具箱构建仿真模型，设计直线轨迹模拟弱非线性工况、圆形轨迹模拟强非线性连续转弯工况，对比扩展卡尔曼滤波（EKF）与无迹卡尔曼滤波（UKF）性能；搭建 PPP-RTK 与 IMU 组合导航测试系统，开展场地试验和丘陵山区验证试验。结果显示，圆形轨迹仿真中，UKF 东向、北向、高程位置误差标准差较 EKF 分别降低 22%、19%、18%；场地试验中 UKF 与真实值重合度显著优于 EKF；田间试验的横向位置最大绝对偏差均值 10.96cm、平均绝对偏差均值 3.08cm、标准差均值 3.02cm，符合作业要求。结果表明，UKF 更适配山区强非线性场景，组合导航系统有助于解决卫星信号遮挡问题，满足农机精细化作业需求。

INTRODUCTION

Navigation and positioning technology is a core technology for intelligent agricultural equipment. It is of great significance for improving the level of agricultural mechanization and realizing precision operation *(Liu et al., 2024)*. Especially in hilly and mountainous areas with complex terrain, traditional agricultural machinery has low operation efficiency due to poor road conditions and significant terrain undulations.

---

[1] *Weisong Zhao, Assistant researcher, Ph.D.; Binxing Xu, Assistant researcher; Chunsong Guan, Associate researcher, Ph.D.; Jia Deng, Professor; Jian Wu, Assistant researcher; Haiyong Ren, Engineer; Jinlong Wang, Engineer; Zhang Shen, Engineer; Chen Zhifeng, Engineer.*

A high-precision and high-reliability navigation system has become a key guarantee for the autonomous operation of agricultural machinery. In recent years, with the rapid development of precision agriculture and intelligent agricultural machinery, navigation and positioning technology has attracted widespread attention in the field of agricultural engineering *(Li et al., 2021; Meng et al., 2023; Shen et al., 2023).*

In terms of GNSS precise positioning, PPP-RTK technology combines the technical advantages of Precise Point Positioning (PPP) and Real-Time Kinematic (RTK). By broadcasting precise orbit, clock bias and regional atmospheric delay correction information, it enables users to achieve rapid ambiguity resolution and centimeter-level positioning accuracy without deploying dense reference stations *(Li et al., 2020; Li, 2021).* In terms of navigation in complex environments, the GNSS/INS integrated navigation system significantly improves the robustness of the system under harsh conditions such as signal occlusion by introducing adaptive filtering methods *(Liu et al., 2016; Zhou et al., 2010; Zhang et al., 2016). Yu et al. (2025)* developed a tightly coupled GNSS/IMU/vision integrated multi-sensor fusion positioning system, and concluded that it can meet the low-cost and high-precision positioning needs of agricultural machinery. *Rottok et al. (2025)* studied a LiDAR-based framework for obstacle identification and mapping in orchard environments, and concluded that this framework can reduce computational requirements, achieve accurate trunk mapping, and provide support for orchard robot navigation and precision agriculture applications. *Gronewold et al. (2025)* researched a tactile sensing and visually-impaired navigation scheme, and concluded that without visual dependence, this system can achieve stable navigation in densely planted row crops and overcome environmental challenges such as row curvature. *Nakaguchi et al. (2024)* studied a machine stereo vision-based navigation system for orchard speed sprayers, and concluded that it can effectively complement the shortcomings of GNSS navigation in orchards and meet the autonomous navigation needs of speed sprayers.

Aiming at the special operation environment of hilly and mountainous areas, scholars have conducted in-depth exploration in fields such as multi-system fusion and vision-aided navigation. *Li et al. (2021)* realized instantaneous ambiguity resolution through multi-frequency and multi-constellation PPP-RTK. In terms of navigation control strategies, the application of sliding mode variable structure control *(Bai et al., 2016),* fuzzy adaptive control *(Jia, 2018)* and improved pure pursuit model *(Han et al., 2018*) has significantly improved the accuracy of path tracking. In addition, navigation research for specific operation platforms such as facility agricultural robots *(He et al., 2024)* and crawler-type harvesters *(Guan, 2020)* has also provided diversified technical solutions for the autonomous operation of agricultural machinery in complex terrain.

Although existing studies have achieved remarkable results in improving the performance of navigation systems, the hilly and mountainous environment still has special technical challenges. Terrain undulations and vegetation coverage lead to frequent interruptions of satellite signals, and PPP-RTK requires a long re-convergence time after signal recovery. Inertial navigation systems (INS) have rapid error accumulation during independent operation, while the traditional Extended Kalman Filter (EKF) is prone to divergence in dynamic scenarios with strong nonlinearity *(Zhou et al., 2010; Xiong, 2017).* In addition, key technologies such as electrification of agricultural machinery chassis *(Zhai et al., 2022)* and steer-by-wire *(Wang et al., 2021)* are still in the development stage, which restricts the further improvement of navigation performance at the system level. Notably, most existing studies focus on open plain areas. The optimization of filtering algorithms for typical terrains such as slopes and curves in hilly and mountainous areas has not been improved, and the systematic verification system from simulation analysis to field tests remains to be established *(Li et al., 2020).* Aiming at the demand for precision navigation of power chassis in hilly and mountainous areas, this study systematically analyzes the estimation performance of Unscented Kalman Filter (UKF) and Extended Kalman Filter (EKF) in nonlinear models, and screens optimized filtering algorithms suitable for strong nonlinear scenarios. By constructing a PPP-RTK/IMU tight-integration navigation system, this study verifies its positioning stability and accuracy in hilly and mountainous areas, in order to provide theoretical support and practical reference for the engineering application of agricultural machinery integrated navigation systems in hilly and mountainous areas.

MATERIALS AND METHODS

Composition of the PPP-RTK and IMU integrated navigation and positioning scheme

Scheme composition

The PPP-RTK and IMU integrated navigation system focuses on wide-area high-precision positioning and autonomous inertial blind compensation, and is suitable for the operation needs of power chassis in hilly and mountainous areas. It mainly consists of a PPP-RTK receiver, an IMU module, and a data acquisition and processing unit.

The PPP-RTK receiver adopts the Huinong MC5 intelligent control integrated machine, which is a highly integrated controller launched by UniStrong Company. It integrates a GNSS antenna, a GNSS receiver, a control unit, WIFI and Bluetooth modules, etc. It can receive GNSS signals of all constellations and frequency bands, and fully supports the reception of BDS-3 satellite signals. It supports multiple differential modes, including RTK, DGNSS, SBAS, and satellite-based differential, which can meet various positioning accuracy requirements such as meter-level, centimeter-level, and millimeter-level.

The IMU module uses the ADIS16488 Micro-Electro-Mechanical Systems Inertial Measurement Unit (MIMU), which integrates a 3-axis accelerometer (measurement range of ±10g, bias stability of ≤0.1mg) and a 3-axis gyroscope (measurement range of ±250°/s, bias stability of ≤0.1°/h). When the PPP-RTK signal is interrupted, it can maintain short-term positioning and attitude output through inertial calculation. The module is packaged in a metal case, with a vibration resistance level of MIL-STD-883H, which is suitable for the bumpy working conditions of chassis in mountainous areas.

The data acquisition and processing unit is based on the NVIDIA Jetson Xavier NX embedded motherboard. It integrates CAN bus, RS232 serial port, and SPI interface to realize synchronous acquisition of multi-source data. It also integrates a Hall-effect wheel speed sensor (resolution of 0.01m/s, slip rate measurement range of 0~30%) and an electronic inclinometer (accuracy of ±0.01°), which are used to correct the speed accumulation error of the IMU and the attitude deviation caused by the chassis roll, respectively.

Working principle and process

The scheme of the PPP-RTK and IMU integrated navigation system is shown in Figure 1. It mainly includes three important parts: multi-source data acquisition and synchronization, data preprocessing and error suppression, and fusion method and positioning output. Each link is progressive and jointly realizes high-precision continuous navigation.

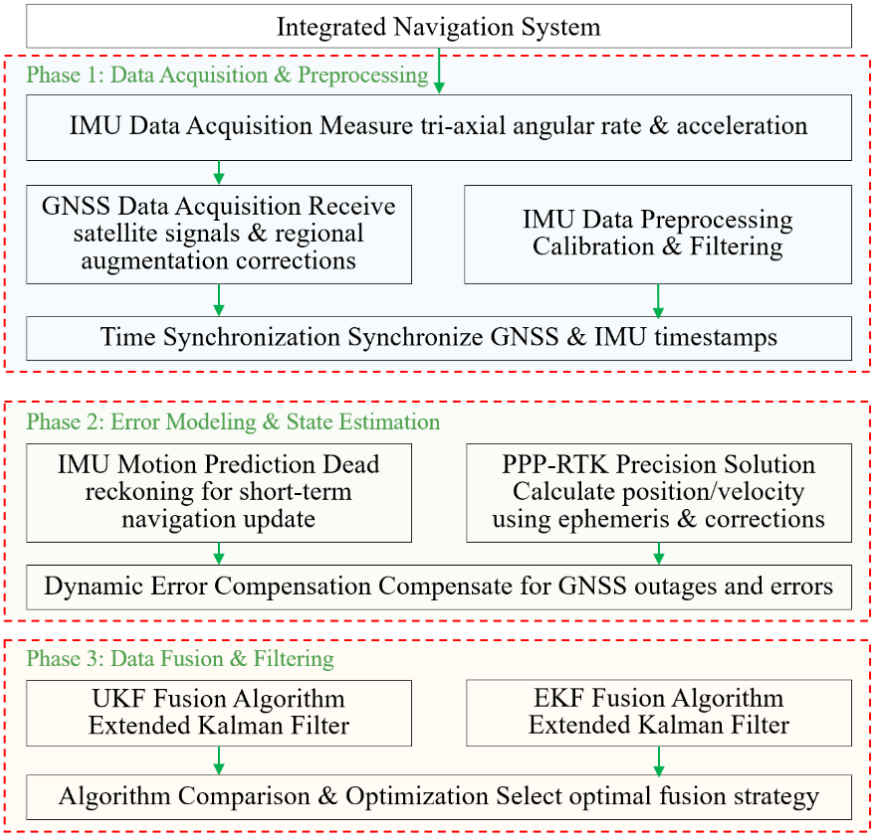

Fig. 1 - PPP-RTK/IMU integrated navigation system scheme

Multi-source data acquisition and synchronization

After the system is powered on, the PPP-RTK receiver receives the Satellite-Based Augmentation System (SBAS) correction data (including satellite orbit/clock bias, ionospheric/tropospheric delay) broadcast by the regional reference network (with a station spacing of 80~100km) through the 4G network. At the same time, the dual-antenna observation outputs the position and heading angle in the geodetic coordinate system, with a data update rate of 1 Hz.

The MIMU outputs the acceleration and angular velocity in the body coordinate system in real time, with a data update rate of 100 Hz. The wheel speed sensor and electronic inclinometer output the chassis driving speed and attitude angle, respectively, with an update rate of 50 Hz.

The data acquisition unit triggers the data sampling of each sensor through the GPS PPS signal, and converts all data to the geodetic coordinate system uniformly. The synchronized multi-source raw data still has environmental interference noise, which is optimized through the data preprocessing and error suppression module in Section 1.2.2 to provide high-quality input for subsequent fusion calculations.

Data preprocessing and error suppression

Aiming at the data noise caused by the complex environment in hilly and mountainous areas, the preprocessing module optimizes the data quality in three steps:

① Outlier elimination: Calculate the deviation between the observed value of each sensor and the historical average. If it exceeds the range (PPP-RTK position deviation > 0.1m, IMU angular velocity deviation > 5°/s), it is determined as an outlier and replaced with the effective value of the previous epoch.

② IMU bias correction: Obtain the initial bias based on static initialization, and update the bias parameters in real time through UKF state estimation during the dynamic process to compensate for the temperature drift and vibration interference of the MIMU.

③ PPP-RTK ambiguity resolution: A prediction model is established using the atmospheric delay observation values of the previous 10 epochs. After the signal occlusion is recovered, the un-differenced ambiguity resolution can be completed within 1 epoch, with a short re-convergence time.

The preprocessed PPP-RTK precise observations, IMU inertial data, and auxiliary sensor information realize the complementarity of multi-source information through the fusion method, and finally output the positioning and attitude results that meet the operation needs of the chassis.

Fusion method and positioning output

Based on the IMU inertial calculation and constrained by the PPP-RTK observation, the optimal fusion of multi-source information is realized through UKF:① Time update: Based on the acceleration and angular velocity of the IMU, the state vector X is updated through the Strapdown Inertial Navigation System (SINS) algorithm, and the system equation $X_k|_{k-1} = f(X_{k-1}|_{k-1}, u_{k-1}) + w_{k-1}$ is constructed, where u_{k-1} is the IMU observation input and w_{k-1} is the system noise.② Measurement update: The position/heading angle of PPP-RTK, the speed of the wheel speed sensor, and the attitude angle of the electronic inclinometer are used as measurement values. The measurement equation is constructed, and the Kalman gain is calculated to update the state vector and covariance matrix, so as to obtain the optimal positioning result. ③ Positioning output: The fusion system outputs the position, speed, and attitude angle in the geodetic coordinate system, with an update rate of 100 Hz. It is transmitted to the drive-by-wire system through the CAN bus to realize the precise path tracking of the power chassis in mountainous areas.

Design and algorithm of Kalman filter

Kalman filter is not only a filter, but also a state estimation method. The core elements of Kalman filter are shown in Figure 2, which mainly include five parts: state vector and its covariance, system model, observation vector and its covariance, observation model, and filtering algorithm.

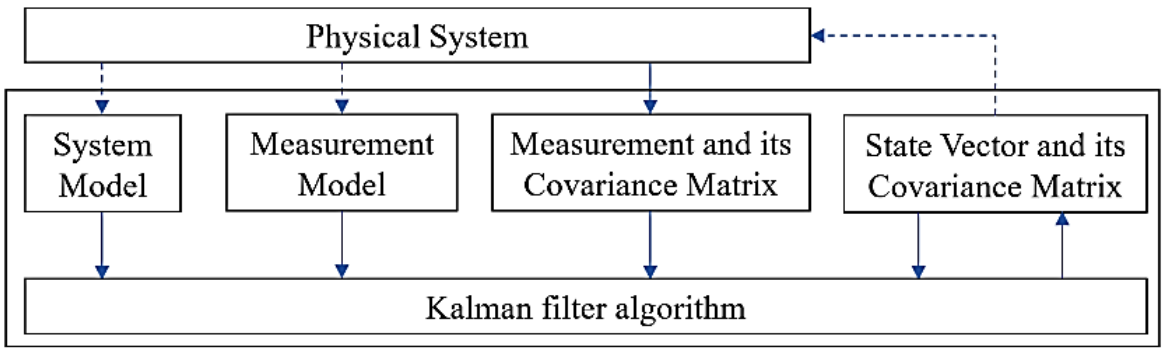

Note: Solid lines indicate data flow that always exists; dashed lines indicate data flow that only exists in certain applications.

Fig. 2 - Core elements of Kalman filter

Basic model of filter

State vector

The state vector is one of the core elements of Kalman filter, as shown in Equation (1). It is a set of observed values of system characteristics at the same time and a function of the state vector.

$$\mathbf{X}_k = \left[x_k,\ y_k,\ z_k,\ v_{x,k},\ v_{y,k},\ v_{z,k},\ \phi_k,\ \theta_k,\ \psi_k,\ b_{a_x,k},\ b_{a_y,k},\ b_{a_z,k},\ b_{g_x,k},\ b_{g_y,k},\ b_{g_z,k} \right]^{\mathrm{T}} \quad (1)$$

In the equation: (x_k, y_k, z_k) is the position in the coordinate system (m); ($v_{x,k}$, $v_{y,k}$, $v_{z,k}$) is the velocity (m/s); (ϕ_k,θ_k,ψ_k) are the roll angle, pitch angle, and yaw angle (rad); b_{a*} and b_{g*} are the IMU accelerometer bias (m/s²) and IMU gyroscope bias (rad/s), respectively. This state vector covers the core physical quantities of chassis navigation (position, velocity, attitude, and sensor bias). It is a key object to be estimated and corrected by subsequent EKF and UKF algorithms, and its accuracy directly determines the operation performance of the navigation system in hilly and mountainous areas.

Observation Vector

The observation vector is shown in Equation (2).

$$\mathbf{Z}_k = \left[x_{\mathrm{ppp},k},\ y_{\mathrm{ppp},k},\ z_{\mathrm{ppp},k},\ \psi_{\mathrm{ppp},k},\ v_{\mathrm{wh},k},\ \phi_{\mathrm{inc},k},\ \theta_{\mathrm{inc},k} \right]^{\mathrm{T}} \quad (2)$$

In the equation: ($x_{ppp,k}$, $y_{ppp,k}$, $z_{ppp,k}$) is the PPP-RTK calculated position (m); $\psi_{ppp,k}$, is the PPP-RTK yaw angle (rad); $v_{wh,k}$ is the wheel speed sensor speed (m/s); ($\phi_{inc,k}$,$\theta_{inc,k}$) are the attitude angles (rad). The observation vector integrates the high-precision positioning information of PPP-RTK and real-time data of auxiliary sensors. It will provide an observation basis for the measurement update stage of EKF and UKF, and realize state error correction by comparing with the state vector.

Extended Kalman filter (EKF) algorithm

The core of EKF is to linearize nonlinear systems through first-order Taylor expansion. It is suitable for weak nonlinear scenarios such as straight-line operation in hilly and mountainous areas.

State prediction

The state is updated based on the IMU inertial navigation model to realize short-term calculation when there is no GNSS observation. The state prediction model is shown in Equation (3):

$$\begin{cases} \hat{X}_{k|k-1} = f\left(\hat{X}_{k-1|k-1}, u_{k-1}\right) \\ P_{k|k-1} = A_{k|k-1} P_{k-1|k-1} A_{k|k-1}^{\mathrm{T}} + Q_{k-1} \end{cases} \quad (3)$$

In the equation: $\hat{X}_{k|k-1}$ is the state prediction value at time k; $f(\cdot)$ is the system nonlinear model; u_{k-1} is the IMU observation value at time k-1 (acceleration a_{k-1}, angular velocity w_{k-1}); $\mathbf{A}_{k|k-1} = \dfrac{\partial \mathbf{f}}{\partial \mathbf{X}}\Big|_{\mathbf{X}_{k-1|k-1}}$ is the system Jacobian matrix; $\mathbf{P}_{k|k-1}$ is the state covariance prediction value; Q_{k-1} is the system noise covariance matrix at time k-1.

Combined with the observations of PPP-RTK and auxiliary sensors, the state prediction error (such as IMU cumulative drift) is corrected, as shown in Equation (4):

$$\begin{cases} v_k = Z_k - h\left(X_{k|k-1}\right) \\ K_k = P_{k|k\text{-}1} H_k^T \left(H_k P_{k|k\text{-}1} H_k^T + R_k\right)^{-1} \\ X_{k|k} = X_{k|k-1} + K_k v_k \\ P_{k|k} = \left(I - K_k H_k\right) P_{k|k-1} \end{cases} \quad (4)$$

In the equation: v_k is the measurement residual; $h(\cdot)$ is the measurement nonlinear model; $H_k = \dfrac{\partial h}{\partial X}\Big|_{X_{k|k-1}}$ is the measurement Jacobian matrix; K_k is the Kalman gain; R_k is the measurement noise covariance matrix at time k; I is the identity matrix; $X_{k|k}$ and $P_{k|k}$ are the state estimation value and covariance matrix at time k, respectively.

This equation uses the high-precision observations of PPP-RTK and auxiliary sensor data to correct the state prediction error, offset the cumulative drift of IMU, and ensure positioning accuracy in weak nonlinear scenarios such as straight-line operation.

Classical unscented Kalman filter (UKF) algorithm

UKF approximates the probability distribution of nonlinear systems through Unscented Transformation (UT transformation). It does not require linearization, avoids the linearization error of EKF, and is more suitable for strong nonlinear working conditions such as continuous turning and steep slopes in hilly and mountainous areas.

The Sigma point propagation and state prediction equations are shown in Equation (5). Through Sigma point propagation and state correction (Equation (6)), measurement update is realized.

$$\begin{cases} \boldsymbol{\chi}^{*}_{i,k|k-1} = \mathbf{f}\left(\boldsymbol{\chi}_{i,k-1|k-1}, \mathbf{u}_{k-1}\right) \quad (i = 0,1,\ldots,2n) \\ \mathbf{X}_{k|k-1} = \sum_{i=0}^{2n} W_i^{(m)} \boldsymbol{\chi}^{*}_{i,k|k-1} \\ \mathbf{P}_{k|k-1} = \sum_{i=0}^{2n} W_i^{(c)} \left(\boldsymbol{\chi}^{*}_{i,k|k-1} - \mathbf{X}_{k|k-1}\right)\left(\boldsymbol{\chi}^{*}_{i,k|k-1} - \mathbf{X}_{k|k-1}\right)^{\mathrm{T}} + \mathbf{Q}_{k-1} \end{cases} \tag{5}$$

$$\begin{cases} \mathbf{Z}_{i,k|k-1} = \mathbf{h}\left(\boldsymbol{\chi}^{*}_{i,k|k-1}\right) \quad (i = 0,1,\ldots,2n) \\ \mathbf{Z}_{k|k-1} = \sum_{i=0}^{2n} W_i^{(m)} \mathbf{Z}_{i,k|k-1} \\ \mathbf{P}_{\mathbf{ZZ},k} = \sum_{i=0}^{2n} W_i^{(c)} \left(\mathbf{Z}_{i,k|k-1} - \mathbf{Z}_{k|k-1}\right)\left(\mathbf{Z}_{i,k|k-1} - \mathbf{Z}_{k|k-1}\right)^{\mathrm{T}} + \mathbf{R}_k \\ \mathbf{P}_{\mathbf{XZ},k} = \sum_{i=0}^{2n} W_i^{(c)} \left(\boldsymbol{\chi}^{*}_{i,k|k-1} - \mathbf{X}_{k|k-1}\right)\left(\mathbf{Z}_{i,k|k-1} - \mathbf{Z}_{k|k-1}\right)^{\mathrm{T}} \\ \mathbf{K}_k = \mathbf{P}_{\mathbf{XZ},k}\mathbf{P}^{-1}_{\mathbf{ZZ},k} \\ \mathbf{X}_{k|k} = \mathbf{X}_{k|k-1} + \mathbf{K}_k\left(\mathbf{Z}_k - \mathbf{Z}_{k|k-1}\right) \\ \mathbf{P}_{k|k} = \mathbf{P}_{k|k-1} - \mathbf{K}_k\mathbf{P}_{\mathbf{ZZ},k}\mathbf{K}_k^{\mathrm{T}} \end{cases} \tag{6}$$

The above UT transformation equations approximate the nonlinear distribution, avoid the linearization error of EKF, and are suitable for strong nonlinear working conditions such as continuous turning and steep slopes in hilly and mountainous areas. They can control the attitude angle error within a relatively small range and effectively improve positioning accuracy.

The calculation process of EKF is initialization → time update → measurement update → iteration. The calculation process of UKF is similar to that of EKF, but after initialization, Sigma point generation is required. During time update, Sigma points are propagated through $f(\cdot)$; during measurement update, Sigma points are propagated through $h(\cdot)$.

Integrated positioning tests and result analysis

Simulation tools and data sources

Simulations were conducted using the PSINS (Precision Strapdown Inertial Navigation System) inertial navigation toolbox on the MATLAB platform. The input data included the measured PPP-RTK positioning data and IMU inertial measurement data of the power chassis in hilly and mountainous areas. The PPP-RTK data was collected by the UN210FBD-2.5SD BDS navigation automatic driving system for agricultural machinery produced by UniStrong Company. The IMU data was collected by the ADIS16488 Micro-Electro-Mechanical Systems Inertial Measurement Unit (MIMU), with the accelerometer having a measurement range of ±10g (bias stability ≤0.1mg) and the gyroscope having a measurement range of ±250°/s (bias stability ≤0.1°/h), and a data update rate of 100 Hz. The auxiliary data was collected by a Hall-effect wheel speed sensor and an electronic inclinometer.

Aiming at the core working conditions of "straight-line operation + continuous turning" for power chassis in hilly and mountainous areas, the measured data were divided into two characteristic trajectory segments, covering weak nonlinear and strong nonlinear scenarios. One was straight-line driving with weak nonlinear characteristics, and the other was a circular trajectory, simulating the continuous turning operation scenario with nonlinearity.

Simulation results and analysis

Two filtering algorithms were trained in MATLAB. Straight-line and circular trajectories were fitted as target values, and the errors of EKF and UKF were compared and analyzed. The simulation effect and error of the straight-line trajectory are shown in Figure 3. From Figure 3a, with the ideal straight-line path (Target Line) as the reference, the trajectory after EKF filtering was more scattered, with a larger range of deviation from the target straight line; while the UKF trajectory was more concentrated and closer to the target straight-line path. From Figures 3b and 3c, in the X and Y directions, the fluctuation range of the UKF positioning error was smaller; the positioning error in the Y direction was slightly smaller than that in the X direction.

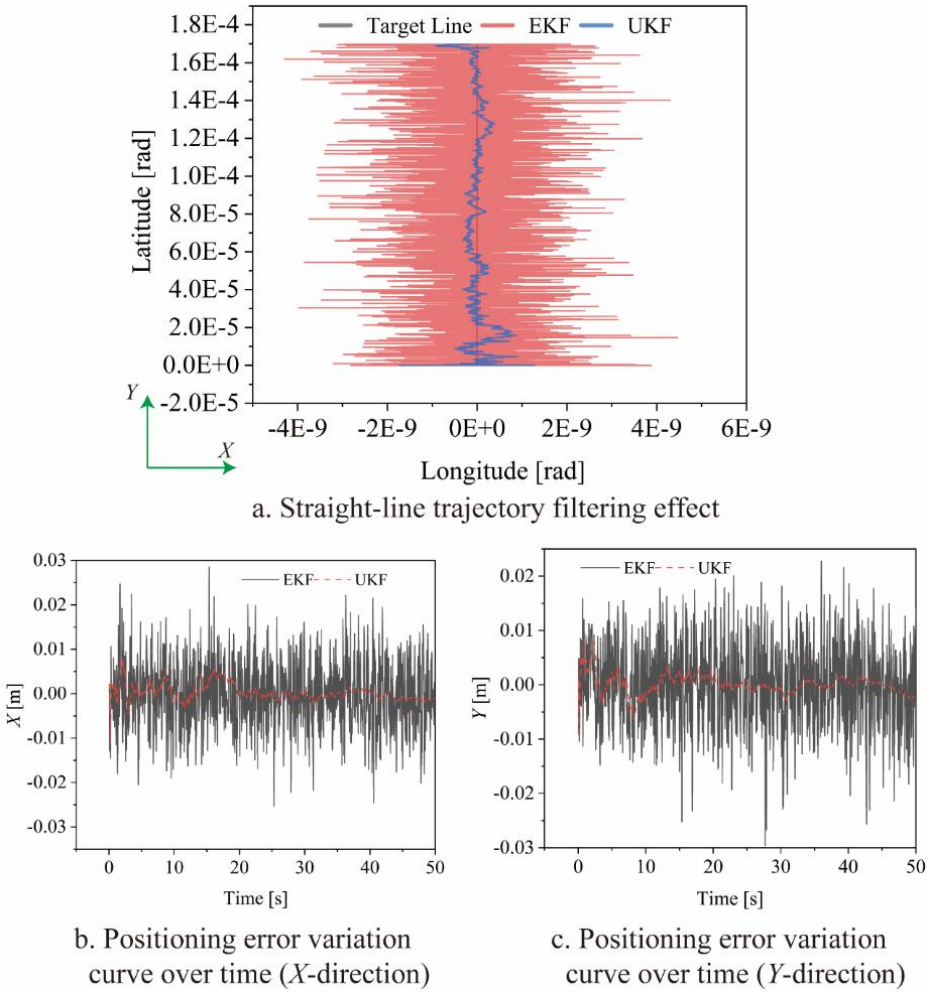

Fig. 3 - Simulation effect and error of straight-line trajectory

The simulation effect and error of the circular trajectory are shown in Figure 4.

From Figure 4a, in terms of altitude, the oscillation amplitude of the EKF-filtered curve was larger, while the UKF-filtered curve was smoother. From Figures 4b and 4c, the error curves of UKF in the X and Y directions were flatter, with fewer error peaks and smaller amplitudes; the EKF error fluctuated sharply, with large errors appearing at multiple time nodes, and its stability was much lower than that of UKF. Under the circular trajectory, the standard deviations of the eastward, northward, and vertical position errors of UKF were reduced by approximately 22%, 19%, and 18% respectively compared with those of EKF. The coincidence degree between the UKF-calculated trajectory and the theoretical path, as well as the dynamic smoothness, were significantly better than those of EKF and single PPP-RTK, effectively avoiding the linearization error of EKF.

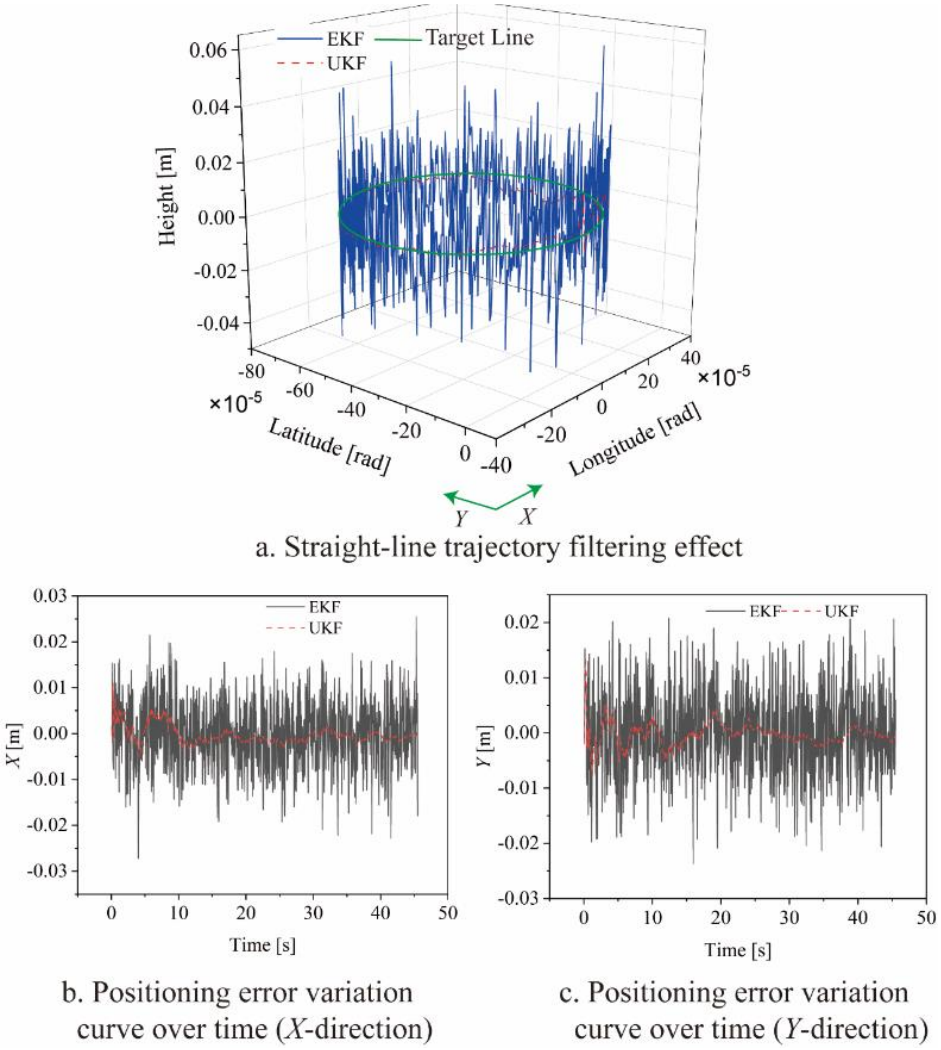

Fig. 4 - Simulation effect and error of circular trajectory

FIELD TESTS

Test equipment

The YZY704 tractor developed by Jiangsu Yueda Intelligent Agricultural Equipment Co., Ltd. was used in the tests. The installed equipment mainly included a GNSS antenna, a radio receiving antenna, an on-board terminal, a controller, an IMU, and an angle sensor. The PPP-RTK data was obtained using the UN210FBD-2.5SD BDS navigation automatic driving system for agricultural machinery (with satellite-based augmentation) produced by Xi'an UniStrong Navigation Technology Co., Ltd. The field tests were carried out in Jiangsu Yueda Intelligent Agricultural Equipment Co., Ltd.

The IMU output 3-axis acceleration information, 3-axis angular velocity information, and tractor attitude information, and was installed at the center of mass of the tractor. The X-axis coincided with the X'-axis, the Y-axis coincided with the Y'-axis, and the direction perpendicular to the module outward was the Z-axis. OXY was the Gauss plane coordinate system, where the X-axis pointed to the coordinate north as positive, and the Y-axis pointed to the coordinate east as positive; the vehicle body coordinate system was a right-hand coordinate system, where the X'-axis pointed to the forward direction of the machine, and the Y'-axis was perpendicular to the forward direction of the machine and pointed to the right side of the driver's seat.

The tests included a straight-line driving test and a tractor continuous turning test (i.e., circular trajectory). During the tests, the path was set through the BDS navigation automatic driving system for agricultural machinery, and the original positioning information of PPP-RTK was recorded. The IMU sensor recorded the original attitude and position information. The data recorded in the tests was sent to the computer via a serial port, and the fused positioning data of PPP-RTK and IMU was obtained through simulation, which was compared and analyzed with the test data.

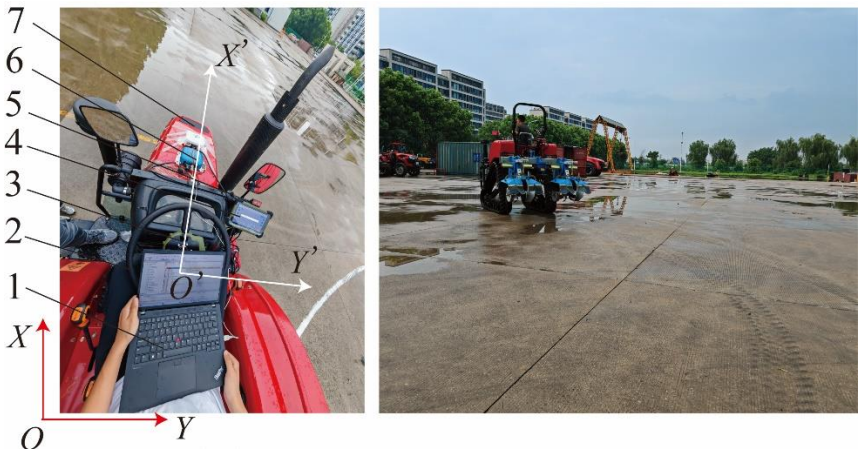

a) Test platform b) Test site

Fig. 5 - Test platform and test site

1. Computer; 2. IMU; 3. Angle sensor; 4. Display screen; 5. Radio antenna; 6. Controller; 7. Tractor

RESULTS AND ANALYSIS

Straight-line driving state

The performance of the positioning and navigation system was tested under the straight-line driving state of the agricultural machinery, and the positioning effects of PPP-RTK and the integrated PPP-RTK/IMU positioning were compared. The test results are shown in Figure 6.

"PPP-RTK" refers to the trajectory under the PPP-RTK navigation and positioning method; "EKF" refers to the result of filtering the integrated PPP-RTK/IMU navigation and positioning using EKF; "UKF" refers to the result of filtering the integrated PPP-RTK/IMU navigation and positioning using UKF. It can be seen from the latitude and longitude trajectory diagram that the UKF-filtered trajectory almost completely coincided with the true value and the PPP-RTK trajectory, with extremely high fitting accuracy; the EKF-filtered trajectory had a slight deviation.

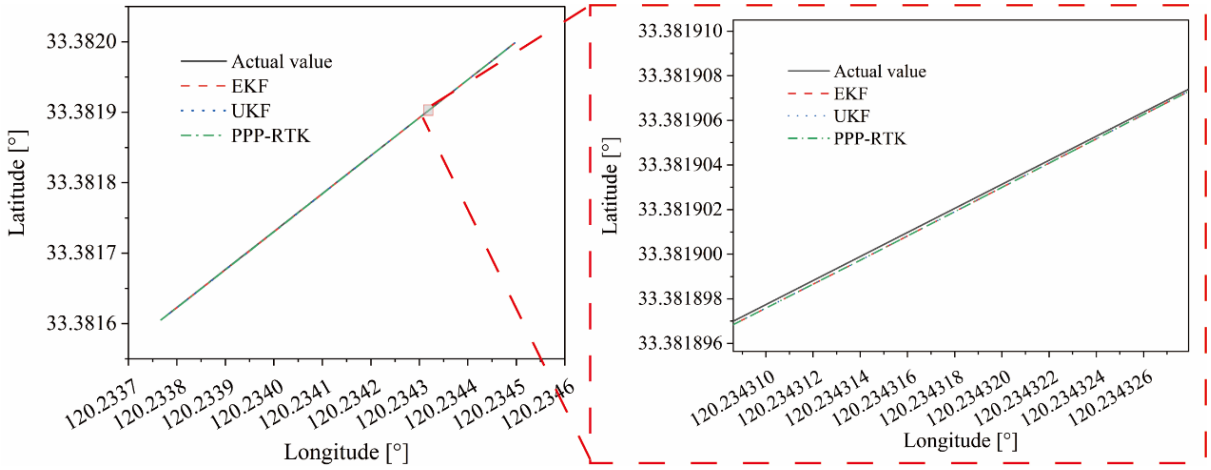

Fig. 6 - Straight line navigation trajectory

The error data in the X and Y directions under the straight-line driving state were extracted, and the results are shown in Figure 7. Figure 7a shows that in the X direction, the error trends of EKF (solid line) and UKF (dashed line) were generally consistent, both showing multi-peak fluctuations. The error peak of EKF was higher, approaching 0.07 m at maximum; the error peak of UKF was relatively lower, and at the valley around 15 seconds, the absolute value of the negative error was smaller. Figure 7b shows that in the Y direction, the error fluctuation amplitude of EKF was larger, with the maximum positive error approaching 0.04 m; the error of UKF was generally flatter, and the absolute values of the peaks and valleys were smaller than those of EKF, and it approached 0 in the later stage. The results show that the maximum errors of UKF in the X and Y directions were both smaller than those of EKF, indicating higher positioning accuracy; the error curve of UKF was flatter, with lower data dispersion, indicating more stable filtering output.

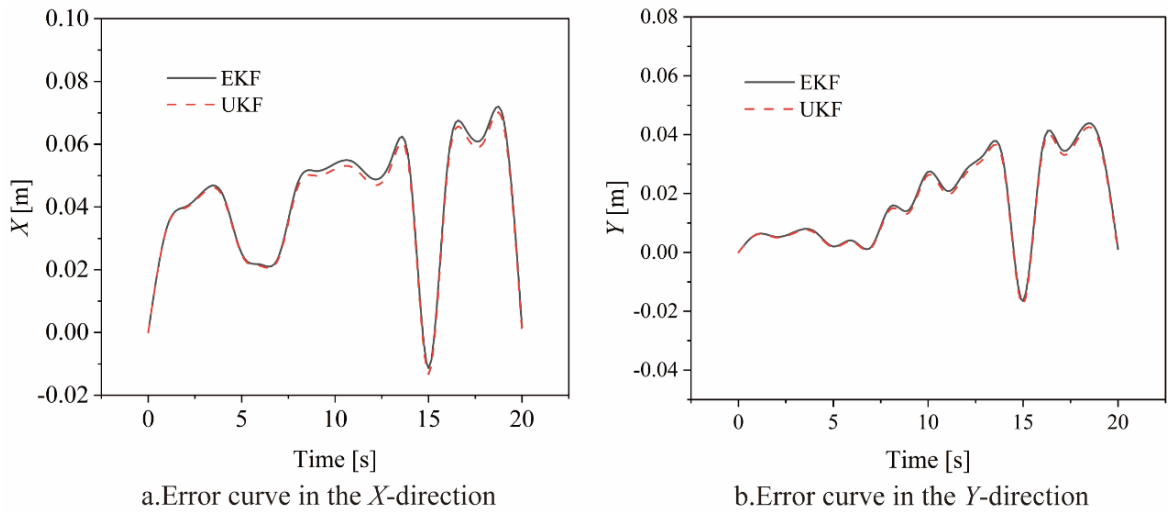

Fig. 7 - Positioning error in straight-line driving

Continuous turning driving state

A test under the continuous turning driving state (i.e., circular trajectory) was carried out to simulate working conditions such as field U-turn and obstacle avoidance. The test results are shown in Figure 8. It can be seen from Figure 8 that the trajectory of EKF (red dotted line) deviated significantly from the theoretical circle, with irregular fluctuations in some parts; the trajectory of UKF (blue dashed line) was closest to the theoretical circle, with an overall smooth shape and high coincidence degree with the reference line; the trajectory of PPP-RTK (green dotted line) was close to the theoretical circle, but its local smoothness was slightly worse than that of UKF.

In terms of trajectory accuracy, the UKF trajectory had the highest coincidence degree with the theoretical circle, and the EKF trajectory had the most obvious deviation. In terms of trajectory consistency, the UKF trajectory was the smoothest overall, without obvious "edges" or fluctuations; the EKF trajectory had large local fluctuations, and the dynamic smoothness of the PPP-RTK trajectory was worse than that of UKF although it was close to the theoretical circle.

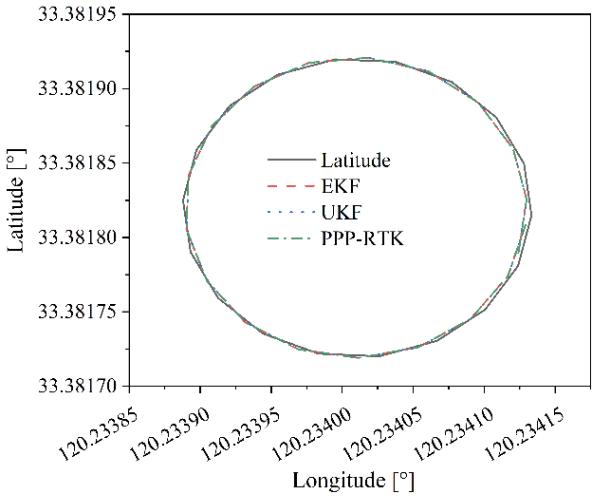

Fig. 8 - Circle line navigation trajectory

The error data in the X and Y directions under the continuous turning driving state were extracted, and the results are shown in Figure 9. Figure 9a shows that in the X direction, the error trends of EKF and UKF were consistent, but the fluctuation amplitude of EKF was larger. The valley value of EKF was close to -0.03 m, and the peak value exceeded 0.01 m in the later stage; the absolute value of the UKF error was significantly smaller, the curve was generally flatter, and the fluctuation range was much smaller than that of EKF. Figure 9b shows that in the Y direction, the UKF curve had higher smoothness.

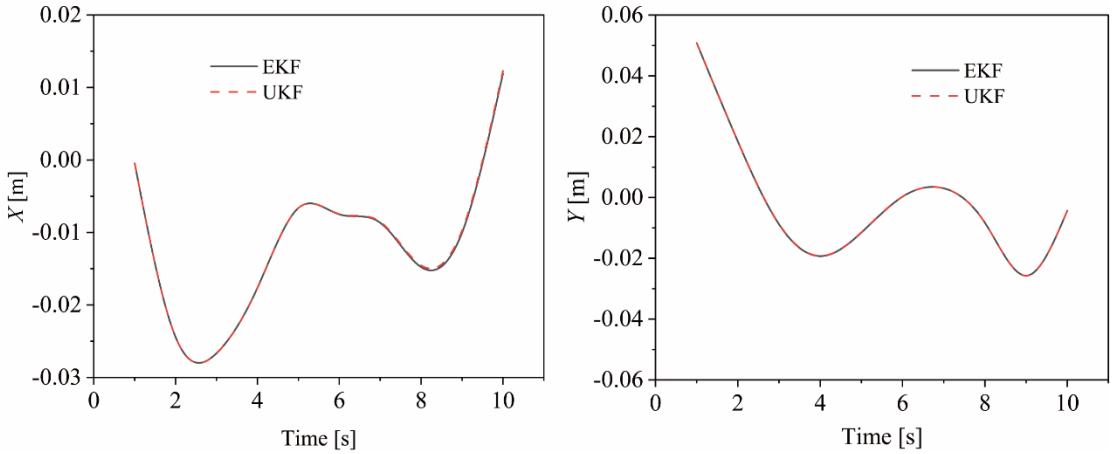

Fig. 9 - Positioning error in circle-line driving

The above test results show that the performance of the PPP-RTK/IMU integrated navigation with the UKF algorithm was significantly better than that with the EKF algorithm. Compared with the single PPP-RTK positioning, the UKF-based integrated navigation had better trajectory smoothness and dynamic consistency, which could effectively improve the navigation accuracy and stability in complex motion scenarios.

Field verification test

To verify the positioning effect of the PPP-RTK/IMU integrated navigation with the UKF algorithm, a field test was carried out on May 26, 2025, in the tobacco planting base of Dejiang County, Tongren City, Guizhou Province. The test area was a typical hilly and mountainous area, with several hills scattered around. The soil was soft, relatively moist, and had a certain stickiness. The test operation site is shown in Figure 10a. During the test, straight-line driving was adopted, with a forward speed of 0.5 m/s. The test was conducted with reference to the standard T/CAAM14-2018 (General Technical Specifications of Auto Steering System for Agricultural Machinery), and statistical analysis was performed on the maximum absolute lateral position deviation, mean absolute deviation, and standard deviation of the straight-line segment. The maximum absolute lateral position deviation and mean absolute deviation reflect the control accuracy, and the standard deviation reflects the control stability. The test results and the test site are shown in Figure 10b. The test was repeated 5 times, and the statistical results are shown in Table 1.

Table 1

Lateral deviations results of field tests

No	Maximum deviation [cm]	Mean absolute deviation [cm]	Standard deviations [cm]
1	11.6	2.7	3.4
2	12.5	4.6	3.7
3	10.4	2.5	2.2
4	11.8	3.3	3.9
5	8.5	2.3	1.9
Average	**10.96**	**3.08**	**3.02**

It can be seen from Table 1 that in the 5 tests, the maximum absolute deviation ranged from 8.5 cm to 12.5 cm (with an average of 10.96 cm), the mean absolute deviation ranged from 2.3 cm to 4.6 cm (with an average of 3.08 cm), and the standard deviation ranged from 1.9 cm to 3.9 cm (with an average of 3.02 cm). In terms of control accuracy, the average value of the maximum absolute deviation did not exceed the lateral deviation tolerance threshold for agricultural machinery operation in hilly and mountainous areas, and the average value of the mean absolute deviation was much lower than the maximum absolute deviation, with a single test value ≤4.6 cm, meeting the requirements of refined agricultural machinery operation.

In terms of control stability, the average value of the standard deviation was small, and there was no obvious "sudden change" in deviation, which indicates that the UKF algorithm can effectively fuse positioning and dynamic attitude information, suppress environmental interference, and ensure strong consistency of the system output. In conclusion, the control accuracy and stability of the integrated navigation system in the complex hilly environment met the standards, which verified the effectiveness of the UKF algorithm and could provide technical reference for high-precision navigation of agricultural machinery in hilly and mountainous areas.

a) Field navigation test site b) Testing at the site with results

Fig. 10 - Field test scenario in hilly and mountainous areas

CONCLUSIONS

Aiming at the problem that single satellite navigation is prone to terrain occlusion and signal interruption, leading to insufficient positioning accuracy and stability when the power chassis operates in hilly and mountainous areas, this study proposed an integrated navigation and positioning scheme with deep fusion of PPP-RTK and inertial measurement unit (IMU). It conducted Kalman filter algorithm design, system hardware integration, simulation analysis, and field and field test verification, and on this basis, constructed an integrated navigation system suitable for complex working conditions in mountainous areas. The main research conclusions are as follows:

(1) Two fusion algorithms, Extended Kalman Filter (EKF) and Unscented Kalman Filter (UKF), were designed. Comparative analysis showed that UKF is more suitable for strong nonlinear operation scenarios in hilly and mountainous areas. A simulation model was constructed using the MATLAB/PSINS toolbox, and field tests were carried out with the YZY704 tractor as the platform. Under the circular trajectory, the standard deviations of the eastward, northward, and vertical position errors of UKF were reduced by 22%, 19%, and 18% respectively compared with those of EKF; the coincidence degree between the UKF-calculated trajectory and the theoretical path, as well as the dynamic smoothness, were significantly better than those of EKF and single PPP-RTK, effectively avoiding the linearization error of EKF.

(2) The results of field tests in hilly and mountainous areas showed that the average value of the maximum absolute lateral position deviation of the system was 10.96 cm, and the average value of the mean absolute deviation was 3.08 cm. The system complies with T/CAAM14-2018 General Technical Specifications for Agricultural Machinery Automatic Navigation Systems and meets the requirements for refined operation of agricultural machinery in hilly and mountainous areas.

ACKNOWLEDGEMENT

This study was supported by the National Key R&D Program of China [Grant Number 2024YFD2300705-03], the China National Tobacco Corporation (CNTC) “Unveiling and Commanding” Project [Grant Number 110202301015], and the Nanjing Modern Agricultural Equipment and Technology Innovation Demonstration Project [Grant Number 2023-07].

REFERENCES

[1] Bai, X. P., Hu, J. T., Zhang, T., (2016). A sliding-mode variable-structure controller based on exact feedback linearization for automatic navigation system. *International Journal of Agricultural and Biological Engineering,* 9(5), pp.158-165.

[2] Guan, Z. H., (2020). *Research on key technologies of auxiliary navigation system for crawler rice combine harvester (履带式水稻联合收获机辅助导航系统关键技术研究)* [PhD dissertation], Hua Zhong Agricultural University, Wuhan/China.

[3] Gronewold, A. M., Mulford, P., Ray, E., Ray, L. E., (2025). Tactile sensing & visually-impaired navigation in densely planted row crops, for precision fertilization by small UGVs. *Computers and Electronics in Agriculture*, 231, 110003.

[4] Han, S. F., He, Y., Fang, H., (2018). Recent development in automatic guidance and autonomous vehicle for agriculture: A Review. *Journal of Zhejiang University (Agriculture and Life Sciences)*, 44(4), pp.381-391.

[5] He, Y., Huang, Z. Y., Yang, N. Y., Li, X. Y., Wang, Y. W., Feng, X. P., (2024). Research progress and prospects of key technologies for facility agricultural robot navigation (设施农业机器人导航关键技术研究进展与展望). *Smart Agricultural*, 6(5), pp.1-19. Beijing/China.

[6] Jia, Q., (2018). *Adaptive control method for tractor auto-guidance system.* (拖拉机自动导航系统自适应控制方法研究). PhD dissertation, Chinese Academy of Agricultural Mechanization Sciences, Beijing/China.

[7] Li, X., (2021). *Research on the key technologies of multi-frequency and multi-constellation GNSS rapid precise positioning* (多频率多星座 GNSS 快速精密定位关键技术研究). [PhD dissertation], Wuhan University, Wuhan/China.

[8] Li, Z. L., Liu, X. F., Chen, X. K., Gao. Y. S., Yang, S. J., (2020). Tractor integrated navigation and positioning system based on data fusion (基于信息融合的拖拉机组合导航定位系统研究) *Transactions of the Chinese Society for Agricultural Machinery*, 51(08), pp.382-390+399. Beijing/China.

[9] Liu, H. L., Shen, C., Hu, L. L., Chang C., Cao, G. Q., (2024). Research progress and development trend of electric agricultural equipments (电动农业装备研究进展与发展趋势). *Transactions of the Chinese Society of Agricultural Engineering*, 40(23), pp.39-51. Beijing/China.

[10] Liu, J. Y., Du, Y. F., Zhang, S., Zhu, Z. X., Mao, E. R., Chen, Y., (2016). Automatic navigation method for agricultural machinery based on GNSS/MIMU/DR information fusion (基于 GNSS/MIMU/DR 信息融合的农业机械自动导航方法). *Transactions of the Chinese Society for Agricultural Machinery*, 47(S1.), pp.1-7. Beijing/China.

[11] Li, Y. B., Zhu, S. P., Wang, J., (2021). Integrated navigation method of electric forklift based on improved ukf algorithm. *INMATEH - Agricultural Engineering*, 65(3), 505-515. Bucharest/Romania.

[12] Luo, X. W., Zhang, Z. G., Zhao, Z. X., Chen, B., Hu, L., Wu, X. P., (2009). Design of DGPS navigation control system for Dongfanghong X-804 tractor (东方红 X-804 拖拉机 DGPS 导航控制系统设计). *Transactions of the Chinese Society of Agricultural Engineering*, 25(11), pp.139-145. Beijing/China.

[13] Meng, Z. J., Wang, H., Fu, W. Q., Liu, M. N., Yin, Y. X., Zhao, C. J., (2023). Research status and prospects of agricultural machinery autonomous driving (农业装备自动驾驶技术研究现状与展望). *Transactions of the Chinese Society for Agricultural Machinery*, 54(10), pp.1-24. Beijing/China.

[14] Nakaguchi, V. M., Abeyrathna, R. M. R. D., Liu, Z., Noguchi, R., Ahamed, T., (2024). Development of a machine stereo vision-based autonomous navigation system for orchard speed sprayers. *Computers and Electronics in Agriculture*, 227, 109669.

[15] Qiao, N., Wang, W., Zhu, X., Tang X., Jin C., Yaoming L., Xu L. (2020). An improved path-tracking controller with mid-angle adaptive calibration for combine harvester. *Journal of Instrumentation*, 15(1):P01025.

[16] Rottok, L. T., Zhou, J., Wang, Y. D., Jiang, Z. Z., Gemechu, T. T., Syed, T. N., Aurangzaib, M, Chepkemoi, M., (2025). Development of a LiDAR-based framework for obstacle identification and mapping in orchard environments. *Biosystems Engineering*, 257, 104245.

[17] Shen, Y., Zhang, Y. F., Liu, H., He, S. W., Feng, R., Wan, Y. L., (2023). Research review of agricultural equipment automatic control technology (农业装备自动控制技术研究综述). *Transactions of the Chinese Society for Agricultural Machinery*, 54(8), pp.1-18.

[18] Wang, W. W., Chen, L. Q., Yang, Y., Liu, L. C., (2021). Development and prospect of agricultural machinery chassis technology (农业机械底盘技术研究现状与展望). *Transactions of the Chinese Society for Agricultural Machinery*, 52(8), pp.1-15.

[19] Xiong, B., (2017). *Research on navigation control method of tractor based on RTK-BDS and DR* (基于RTK-BDS和DR的拖拉机导航控制方法研究). [PhD dissertation], China Agricultural University. Beijing/China.

[20] Yu, J., Fang, H., Zhang, X., Wu Wentao, He Yong. (2025). Tightly coupled GNSS/IMU/vision integrated system for positioning in agricultural scenarios. *Computers and Electronics in Agriculture*, 239, 110478.

[21] Zhai, C. Y., Yang, S., Wang, X., Zhang, C. F., Song, J., (2022). Status and prospect of intelligent measurement and control technology for agricultural equipment (农机装备智能测控技术研究现状与展望). *Transactions of the Chinese Society for Agricultural Machinery*, 53(4), pp.1-20.

[22] Zhang, S., Du, Y. F., Zhu Z. X., Mao, E. R., Liu, J. Y., Shi, J., (2016). Integrated control method of traction & slip ratio for rear-driving high-power tractors (后轮驱动大功率拖拉机牵引力-滑转率联合自动控制方法). *Transactions of the Chinese Society of Agricultural Engineering*, 32(12), pp.47-53. Beijing/China.

[23] Zhong, Y., Xue, M. Q., Yuan, H. L., (2021). Design of the GNSS/INS integrated navigation system for intelligent agricultural machinery (智能农机 GNSS/INS 组合导航系统设计) *Transactions of the Chinese Society of Agricultural Engineering*, 37(9), pp.40-46. Beijing/China.

[24] Zhou, J., Zhang, P., Liu, C. L., (2010). Kalman filtering for integrated navigation based on time series analysis (基于时间序列分析的卡尔曼滤波组合导航算法). *Transactions of the Chinese Society of Agricultural Engineering*, 26(12), pp.254-258. Beijing/China.